Profiling Cas9-and Cas12a-induced mutagenesis in Arabidopsis thaliana

Pater, S. de; Kamoen, L.; Schendel, R. van; Hooykaas, P.J.J.; Tijsterman, M.

the plant journal

SEB SOCIETY FOR EXPERIMENTAL BIOLOGY

The Plant Journal (2024) **119,** 2706–2717 doi: 10.1111/tpj.16943

Profiling Cas9- and Cas12a-induced mutagenesis in *Arabidopsis thaliana*

Sylvia de Pater[1], Lycka Kamoen[1], Robin van Schendel[2], Paul J. J. Hooykaas[1] and Marcel Tijsterman[1,2,*]
[1]*Department of Plant Sciences, Institute of Biology, Leiden University, Leiden, BE 2333 the Netherlands, and*
[2]*Department of Human Genetics, Leiden University Medical Center, Leiden, RC 2300 the Netherlands*

Received 28 May 2024; revised 10 July 2024; accepted 13 July 2024; published online 25 July 2024.
*For correspondence (e-mail m.tijsterman@lumc.nl).

SUMMARY

With the advancement of CRISPR technologies, a comprehensive understanding of repair mechanisms following double-strand break (DSB) formation is important for improving the precision and efficiency of genetic modifications. In plant genetics, two Cas nucleases are widely used, i.e. Cas9 and Cas12a, which differ with respect to PAM sequence composition, position of the DSB relative to the PAM, and DSB-end configuration (blunt vs. staggered). The latter difference has led to speculations about different options for repair and recombination. Here, we provide detailed repair profiles for LbCas12a in *Arabidopsis thaliana*, using identical experimental settings previously reported for Cas9-induced DSBs, thus allowing for a quantitative comparison of both nucleases. For both enzymes, non-homologous end-joining (NHEJ) produces 70% of mutations, whereas polymerase theta-mediated end-joining (TMEJ) generates 30%, indicating that DSB-end configuration does not dictate repair pathway choice. Relevant for genome engineering approaches aimed at integrating exogenous DNA, we found that Cas12a similarly stimulates the integration of T-DNA molecules as does Cas9. Long-read sequencing of both Cas9 and Cas12a repair outcomes further revealed a previously underappreciated degree of DNA loss upon TMEJ. The most notable disparity between Cas9 and Cas12a repair profiles is caused by how NHEJ acts on DSB ends with short overhangs: non-symmetric Cas9 cleavage produce 1 bp insertions, which we here show to depend on polymerase Lambda, whereas staggered Cas12a DSBs are not subjected to fill-in synthesis. We conclude that Cas9 and Cas12a are equally effective for genome engineering purposes, offering flexibility in nuclease choice based on the availability of compatible PAM sequences.

Keywords: Cas12a, Cas9, non-homologous end-joining (NHEJ), polymerase theta-mediated end-joining (TMEJ), DNA polymerase lambda, double strand breaks, *Arabidopsis thaliana*.

INTRODUCTION

In the realm of plant molecular biology, CRISPR-Cas genome editing technologies have emerged as powerful tools for targeted genetic modifications, offering immense potential for crop improvement, trait enhancement, and functional genomics studies (Bortesi & Fischer, 2014; Guo et al., 2023; Li et al., 2024). Among the arsenal of CRISPR-associated nucleases, Cas9 and Cas12a have received most attention (Swartjes et al., 2020), partly due to their efficiency, specificity, and applicability across a wide range of plant species (Capdeville et al., 2021, 2023). Both enzymes are RNA-guided nucleases able to induce double-stranded DNA breaks (DSBs) at specific genomic locations, thereby initiating cellular DNA repair mechanisms (Liu et al., 2023).

The repair of DSBs in plants predominantly occurs through two principal pathways: homology-directed repair (HDR), which offers a precise mechanism for introducing desired genetic modifications, and non-homologous end joining (NHEJ) that often results in small insertions or deletions at the site of the break thus offering a mechanism for gene inactivation. In NHEJ, the DNA binding proteins Ku70 and Ku80 form a complex that binds DSB ends, protecting it from degradation and recruiting the enzymes necessary for ligation (Chang et al., 2017). More recently, it has become clear that another, less prominent, DSB repair pathway is responsible for a significant fraction of CRISPR-induced mutations in a range of species (Schimmel et al., 2019). This pathway critically depends on DNA polymerase theta (Polθ) (Wood & Doublié, 2022) and is

hence called Theta-Mediated End-Joining (Roerink et al., 2014; Ramsden et al., 2022). Although NHEJ is able to very efficiently repair DSBs (blunt and staggered ends) in an accurate manner, thus restoring the original sequence, TMEJ is intrinsically mutagenic: small (2–3 bp) direct repeats present in the flanks of opposing DSB ends are used as minimal primers for Polθ action. This requirement for minimal base pairing prior to DNA synthesis explains the characteristic feature of so-called microhomology (MH) observed at most TMEJ deletion junctions. During TMEJ, for yet unknown reasons, primer template switching occasionally occurs resulting in so-called templated insertions (Schimmel et al., 2019), which in plants is more frequent than in animals likely because plants do not encode HelQ, which was recently shown to suppress the formation of templated insertions (Kamp et al., 2021).

Despite the shared capacity of Cas9 and Cas12a to generate DSBs, recent studies have highlighted variations in the efficiency and fidelity of DNA repair following Cas9 and Cas12a cleavage events (Hur et al., 2016; Kleinstiver et al., 2016; Tang et al., 2017), suggesting potential distinctions in the DNA repair outcomes brought about by these nucleases. Factors such as the sequence context of the target site, the presence of DNA modifications, the retention time of the enzyme after DSB induction, as well as the cell cycle stage or the differentiation state can all influence DNA repair. Moreover, Cas9 and Cas12a generate different DSB configurations: the nuclease activities in Cas9 incises the two DNA strands at an almost equal distance from the PAM sequence thus mostly creating blunt DSB ends with occasionally a 1 bp stagger (Zuo & Liu, 2016; Shou et al., 2018). In contrast, Cas12a cuts DNA in a staggered pattern, where ssDNA incisions are 4–5 bp apart, generating DNA ends having 5′ single-stranded protrusions. These variables may contribute to reported differences in repair fidelity and efficiency between the two CRISPR nucleases. In this study, we aim to systematically compare the DNA repair outcomes and pathways activated by Cas9 and Cas12a in plants, using a combination of experimental methodologies and computational analyses. We have recently provided a high-resolution analysis of repair of Cas9-induced DSBs in *Arabidopsis thaliana* (Kamoen et al., 2024) and here report on DSB repair following Cas12a-induces breaks. To this end, we targeted the same genomic loci and used identical reagents except for an improved, temperature-tolerant variant of Cas12a that was recently shown to be effective in various plant species including *Arabidopsis*, tomato, and rice (Bandyopadhyay et al., 2020; Schindele & Puchta, 2020; Slaman et al., 2024; Zhang et al., 2022).

In this study, we also investigate the biology of integrating externally provided DNA into the genome at sites of Cas12a-induced DSBs. In our experiments, we use *Agrobacterium*-mediated transformation (AMT) to establish expression of the CRISPR reagents in the plant cells. In AMT, a single-strand segment of bacterial DNA, called T-DNA, which is here genetically engineered to encode Cas enzymes and crRNA, is transmitted to plant cells. Upon arrival in the nucleus, these genes are expressed either before (transient expression) or after integration of T-DNA into the plant genome (stable expression). Although these transformation protocols offer opportunities for genomic engineering, they also pose a safety risk, as the DSBs generated by the Cas enzymes can serve as entry points for T-DNA integration. The outcomes of this process can be both desired (to establish transgenesis) and undesired (unwanted integration of CRISPR reagents into host genomes). To discern whether Cas12a and Cas9 promote the integration of exogenously provided DNA into the genome at the targeted site equally or differently, we conducted high-resolution NGS-based analysis across various target sites.

By elucidating the distinct repair mechanisms acting on the DSBs induced by these nucleases in plant genomes, we aim to enhance our understanding of CRISPR-based genome editing in plants and facilitate the development of tailored editing strategies for crop improvement and agricultural biotechnology applications.

RESULTS

Cas12a-induced DSB repair footprints

To provide a comprehensive profile of Cas12a repair outcomes, a temperature-tolerant variant of Cas12a (LbttCas12a) (Schindele & Puchta, 2020) was used to induce DSBs in three different target sites (Figure 1a). The target sites were located in genes encoding Alcohol Dehydrogenase 1 (ADH), Cruciferin 3 (CRU), and Protoporphyrinogen Oxidase (PPO) and were chosen in close proximity to the sites previously used for analyzing Cas9-induced DSB repair (Kamoen et al., 2024).

Wild-type, *ku70*, and *teb* mutant plant lines were transformed with T-DNA encoding the CRISPR reagents. Whereas *ku70* mutant plants are impaired in NHEJ, enabling us to exclusively study TMEJ, *teb* mutant plants are deficient for polymerase theta (Polθ), leaving only NHEJ to facilitate end joining. Three weeks after root transformation, DNA was isolated from pooled calli and subjected to footprint analysis using Illumina amplicon deep sequencing of the target sites. For processing of the data, subsequent analysis, and visualization, we used SIQ (Sequence Interrogation and Quantification) (van Schendel et al., 2022).

Using this approach, we found 13–28% of alleles to be mutated in repair proficient calli (Figure 1b). The majority of mutations were simple deletions (dels) and deletions with embedded insertions (delins); the embedded insertions frequently had stretches of sequence that were

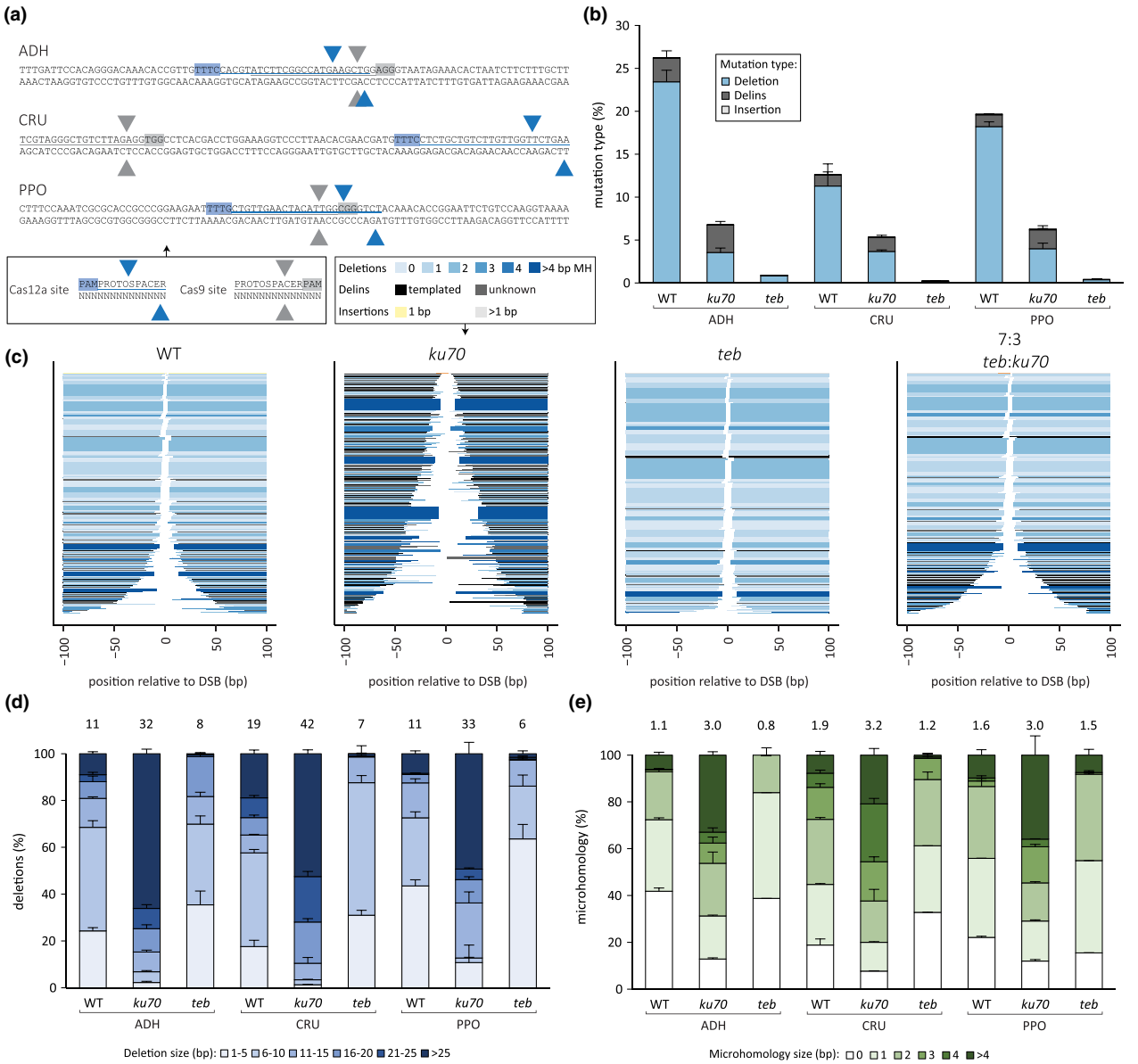

Figure 1. Mutational footprints in the ADH, CRU and PPO locus after Cas12a DSB induction.
(a) Target sites in genes encoding ADH, CRU and PPO. Cas12a targets are blue and Cas9 targets in gray (protospacer are underlined, PAM sites are highlighted and cut sites indicated with triangles).
(b) Percentage and type of mutation in WT, *ku70* and *teb* mutants at ADH, CRU and PPO target sites.
(c) Tornado plots of combined ADH, CRU and PPO targets in wild type, *ku70* and *teb* mutants. All mutational events of combined biological replicates are stacked and sorted based on their deletion size. The frequency of occurrence of each event is represented by the thickness of the respective bar. The events are color coded based on the type of event. The relative position on the x-axis includes the expected DSB position at 0 bp. The *ku70* mutant (second panel) and *teb* mutant (third panel) were combined in a 3:7 ratio (right panel), which accurately fits the spectrum obtained in wild type (left panel).
(d) Microhomology use and (e) deletion size of all deletion events. The error bars represent the standard error between biological replicates.
(d–e) The error bars represent the standard error (SE) between biological replicates. The weighted average of deletion size and microhomology use is indicated on top of the bars.

identical to the flanking sequences, which are thought to have served as a template during TMEJ, and are hence called templated insertions (Schimmel et al., 2019). The non-altered outcomes could reflect uncut alleles or accurate repair (Kamoen et al., 2024). For *ku70* mutant calli, the mutation frequency dropped to around 6% (Figure 1b), while the profile dramatically changed (Figure 1c): deletions were grosso modo larger (Figure 1d; Figure S1) and the degree of microhomology (MH) at the deletion junctions increased (Figure 1e), as also the ratio of delins over deletions (Figure 1b). The DSB repair profile obtained for NHEJ mutant plants is thus entirely consistent with TMEJ

activity (Schimmel et al., 2019). Conversely, the spectrum derived from *teb* mutant calli is reflective of NHEJ repair: deletions are small without obvious microhomology at their junctions, and no delins are generated (Figure 1c–e). Notably, *teb* mutant calli had a very low mutation frequency (0.2–1%, Figure 1b), not because of reduced repair, but because T-DNA integration and subsequent expression of Cas12a is severely compromised in Polθ deficient plant cells and DSB induction thus depends on transient expression of the CRISPR nuclease only (Kamoen et al., 2024). By comparing profiles composed of different ratios of NHEJ and TMEJ outcomes to the profile obtained for wild type, we infer that under genetically non-compromised conditions Cas12a mutations are for 70% produced by NHEJ and for 30% by TMEJ (Figure 1c).

T-DNA capture at Cas12a-induced DSBs

Subsequently, we assayed whether Cas12a can be exploited for targeted integration of T-DNA molecules, to facilitate the development of technology to transform plants in a controlled fashion. Recently, we have reported on a surprisingly high number (8%) of T-DNA being captured at Cas9-induced DNA breaks (Kamoen et al., 2024). We established that the 3′ end of these T-DNA molecules (termed LB for left border) requires TMEJ for becoming attached to a genomic DSB, whereas attachment of the 5′ end (termed RB for right border) can be brought about by both TMEJ and NHEJ. To investigate whether these distinct genetic requirements, as well as the overall effectiveness, are affected by the nature of the genomic DSB, being either blunt ended or not, we analyzed genome-T-DNA junctions in plants transformed with Cas12a CRISPR reagents. To determine the frequency of T-DNA capture, we used CISGUIDE (Kamoen et al., 2024). This method makes use of only one primer binding site at the targeted locus, and uses an adapter approach that provides the other primer binding site. This way, CISGUIDE can identify all DNA sequences that become attached at one end of an inflicted DSB. The joined molecule could be the other break end (in close or distant position) but also another chromosome or T-DNA (Figure 2a). We found 0.9% of amplification products to be genome-T-DNA joints (Figure 2b), representing 3.4% of all mutagenic products, with various segments of the T-DNA being captured: 0.6% of ends are attached to LB, 1.3% to RB, 0.8% to a middle part of the T-DNA and 0.7% to the vector backbone (Figure 2c), which is sometimes transferred to the plant cells linked to the T-DNA (Jupe et al., 2019). Subsequently, we exploited amplicon deep sequencing to establish T-DNA-genome junction profiles (Figure 2a) by making use of combinations of one genomic primer flanking the DSB, and one T-DNA primer close to the LB or RB end (facing outward). In Figure 2d, we have combined the outcomes for both sides of three targets (ADH, CRU and PPO) in Tornado plots. The profile of LB-genome junctions had a characteristic TMEJ signature: frequently containing (templated) insertions (also known as filler-DNA) in between the T-DNA and the genome (Figure 2e) as well as a profound overrepresentation of (simple) junctions containing MH (Figure 2f). Consistent with inferring a role for TMEJ in connecting the LB end of T-DNA to a genomic DSB (Kralemann et al., 2022), the profile was unchanged when NHEJ mutant plants (*ku70*) were analyzed (Figure 2d–h). In contrast, the RB-genome profile markedly changed in *ku70* mutant plants in line with the wild-type profile having outcomes indicative of NHEJ: no fillers, junctions without MH, and minimal loss of both T-DNA and genome sequence (Figure 2d–h).

CISGUIDE and long-read sequencing of Cas9- and Cas12a-induced DSBs

From the data presented in Figure 1, which was derived by short-read Illumina sequencing, it is clear that not all deletion outcomes are captured (Figure 3a): deletions that extend beyond the PCR and sequence primer binding sites will be missed, which may especially impact the profile obtained in NHEJ deficient conditions. To correct for this shortcoming and gain a more comprehensive overview of the degree of sequence loss at sites of DSBs induced by CRISPR, we used two other methods of detection: CISGUIDE and long-read PacBio sequencing (Figure 3b). The afore-described CISGUIDE methodology determines which sequence "ends up" being attached to an inflicted DSB, in an unbiased fashion. Figure 3c shows all mutant alleles induced by both Cas12a and Cas9 for which at least the sequence 70 bp away from the break is retained at one end of the DSB. Confirming our expectation, in the same samples that were analyzed by short read sequencing, we find additional mutant alleles, particularly in NHEJ deficient plants in which TMEJ is monitored. CISGUIDE also allows us to address how many DSB ends are ligated to DNA molecules other than the opposing DSB end. We found 25% of alleles to have undergone DSB repair, 0.9% of alleles to have captured a T-DNA molecule at the target site, whereas 0.4% of alleles were joined to various other parts of the genome, likely representing translocations (Figure 2b).

Subsequently, we conducted long-read sequencing of amplicons of approximately 4 kb, using PacBio. Here, we additionally analyzed calli of wild type and *ku70* plants previously transformed with Cas9 to allow for a direct comparison. Because of the high error rate of PacBio sequencing (which leads to erroneous annotations of repair outcomes as delins instead of deletions) we restricted our analysis to simple deletions (deletions without embedded insertions) and insertions. Figure 3d displays Tornado representations resulting from repair of Cas12a and Cas9-induced DSBs within the PPO target for

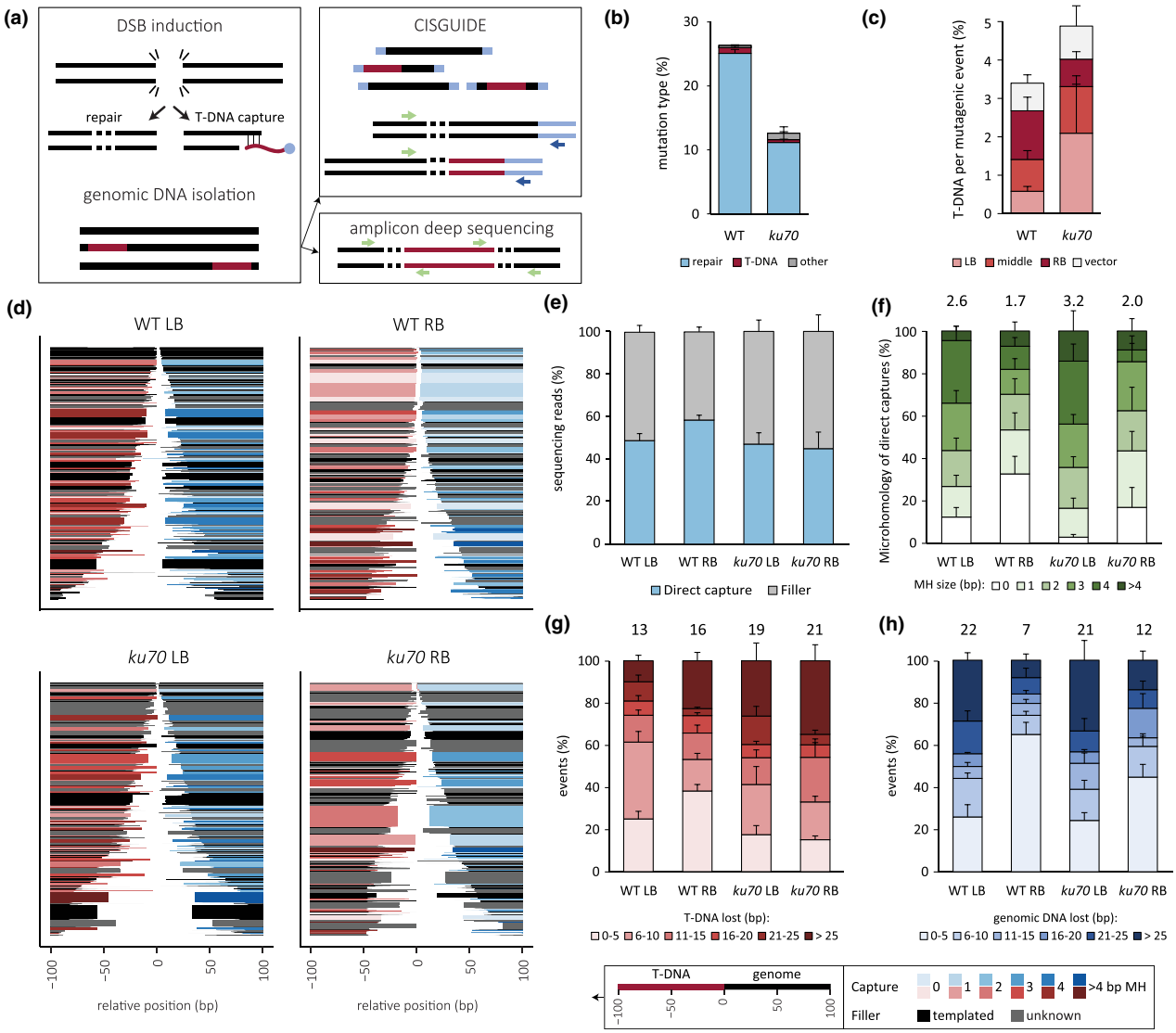

Figure 2. Mutational footprints in junctions between the genome and the T-DNA LB or RB.
(a) Outline of the CISGUIDE and amplicon deep sequencing methods used to identified T-DNA-genomic DNA junctions. A DSB is induced by CRISPR/Cas which may be repaired or T-DNA (red) may be captured at this site. The affected sites were inspected by CISGUIDE and amplicon deep sequencing (right panel). For CISGUIDE (CRISPR-induced Sequence Gain/loss, Unbiased Identification), adapter sequences (blue) are ligated to fragmented genomic DNA, and PCR is performed using a locus specific primer (green), and a primer binding to the adapter (blue). For amplicon deep sequencing of T-DNA capture junctions at the DSB, a locus specific primer (green) was combined with a T-DNA specific primer (green). Libraries of amplicons were subsequently analyzed by NGS.
(b) Percentage of mutagenic sequencing reads as determined by CISGUIDE. Repair indicates the distal end of the sequencing read contained the other flank of the break. T-DNA indicates the distal end contained part of the T-DNA. Other indicates the distal end contained another sequence.
(c) Percentage of T-DNA events normalized for the percentage of mutagenic events depicted in B, divided in location on the T-DNA or binary vector backbone. LB and RB indicate a window of 200 bp around the respective border. Middle indicates any other location on the T-DNA. Vector indicates a position on the binary vector outside of the T region.
(d) Tornado plots of the T-DNA-genome junction for the indicated genotypes and borders, combined for all biological replicates and ADH, CRU and PPO target sites. All mutational events are stacked and sorted based on their deletion size. The frequency of occurrence of each event is represented by the thickness of the respective bar. The events are color coded based on the type of event. The relative position on the x-axis includes the expected T-DNA end and DSB position at 0 bp. Negative values indicate the T-DNA flank (red/gray) and positive values indicate the genomic flank (blue/gray).
(e) Percentages of events with or without filler DNA.
(f) Histogram depicting the microhomology use of all direct capture events.
(g) Histogram depicting the deletion size on the T-DNA flank of all direct capture events.
(h) Histogram depicting the deletion size on the genomic flank of all direct capture events.
(b, c, e–h) The error bars represent the SE between biological replicates.
(f–h) The weighted average of microhomology use and deletion size is indicated on top of the bars.

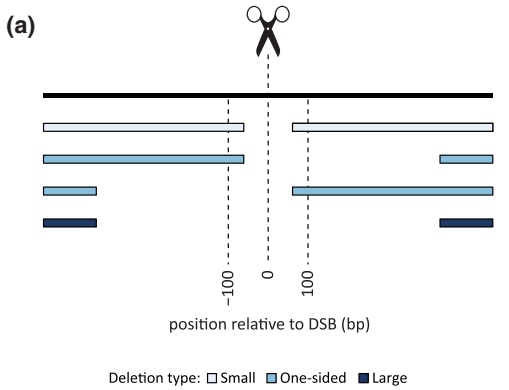

(b)

Deletion type	Detectable with		
	Illumina	CISGUIDE	PacBio
Small	+	+	+
One-sided		+	+
Large			+

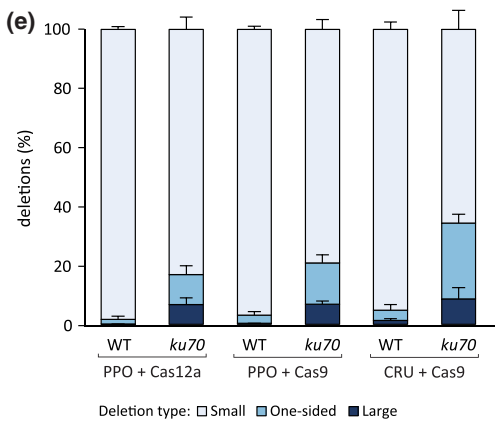

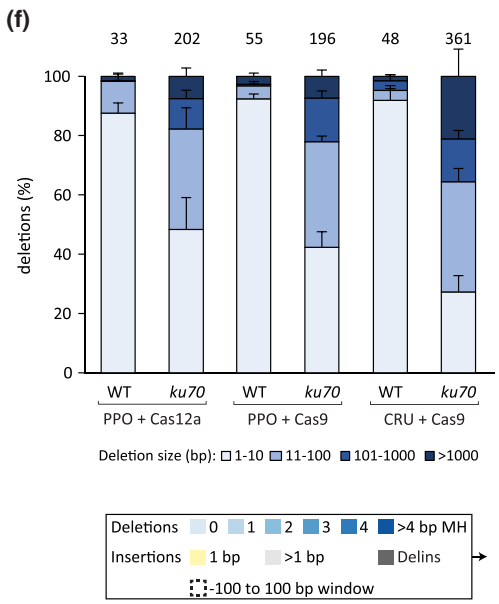

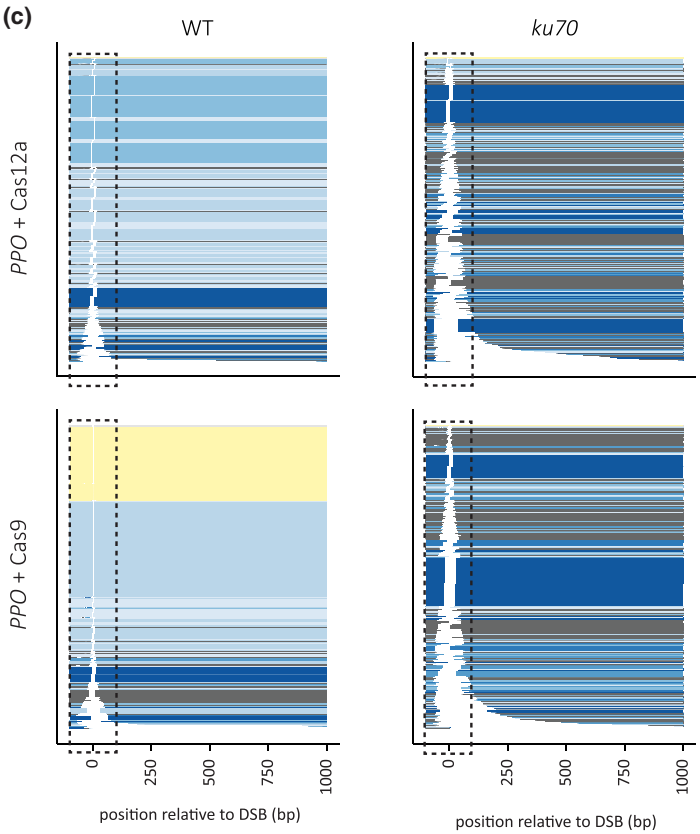

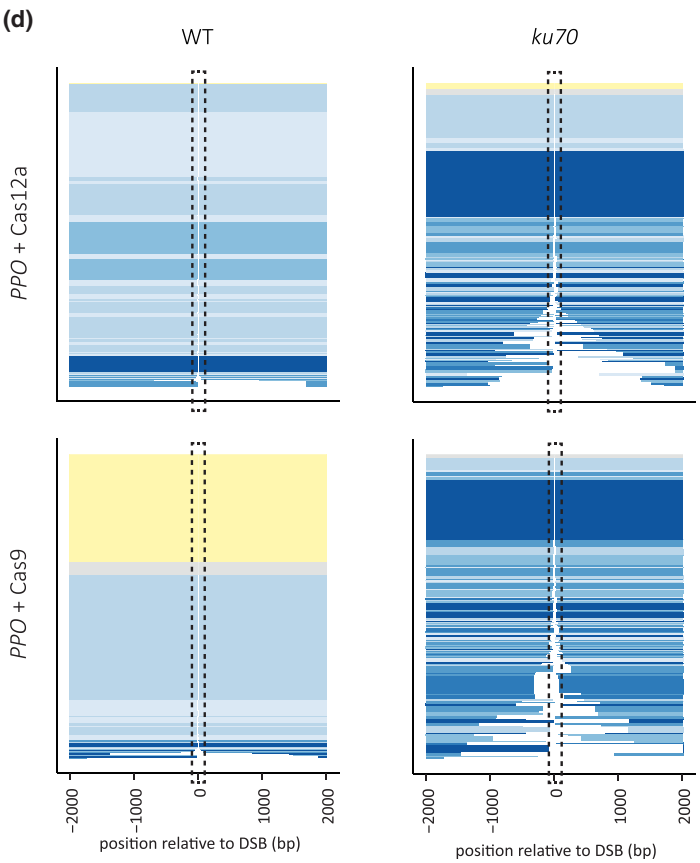

Figure 3. Mutational footprints analyzed by CISGUIDE and PacBio.
(a) Deletions were classified as small, one-sided, and large.
(b) Overview of deletion size detected by Illumina, CISGUIDE and PacBio.
(c) Spectra of mutations of repair footprints of DSBs induced by Cas9 and Cas12a in the PPO target in wild type and *ku70* combined for all biological replicates and both orientations determined by CISGUIDE. The relative position on the *x*-axis includes the expected DSB position at 0 bp. All mutational events are stacked and sorted based on their deletion size. The number of reads representing a specific outcome is represented by the thickness of the respective bar. The events are color-coded based on the type of event and the extent of microhomology (MH). The Cas9 data are from (Kamoen et al., 2024) for comparison. Dashed areas represent outcomes detectable by Illumina.
(d) Tornado plots of repair footprints of DSBs induced by Cas9 and Cas12a in the PPO target in wild type and *ku70* mutants determined by PacBio. All mutational events of combined biological replicates are stacked and sorted based on their size. The frequency of occurrence of each event is represented by the thickness of the respective bar. The events are color coded based on the type of event. The relative position on the *x*-axis includes the expected DSB position at 0 bp. Dashed areas represent outcomes detectable by Illumina.
(e) Small, one-sided, and large deletion class distribution after Cas9 or Cas12a-induced DSB in the PPO or CRU locus in wild type and the *ku70* mutant.
(f) Histogram depicting the deletion size class distribution of all deletion events. The weighted average of the deletion size is indicated on top of the bars. (e, f) The error bars represent the SE between biological replicates.

both wild type and *ku70* genotypes. Very similar results were obtained with Cas9 and the CRU target (Figure S2). Combining the CISGUIDE and long-read sequencing of repair outcomes allow us to draw the following additional conclusions: (i) in wild-type plants, the vast majority of CRISPR-induced mutations are deletions that are smaller than 3 bases (median); (ii) deletions resulting from TMEJ can be substantially larger: 20–40% are not captured in small-read sequencing, and 18–36% of deletions are larger than 100 bp (Figure 3f); (iii) interestingly, also these larger deletions are characterized by micro-homologous junctions (Figure 3c,d), which to us suggest that the molecules that are joined are not full-length when Polθ is engaged; (iv) moreover, many of the larger deletions events have lost the DNA only on one end (see the *ku70* repair profiles shown in Figure 3e, where many of the deletions are non-symmetrical with respect to the DSB). We will later propose a potential explanation for this non-symmetrical repair pattern; and (v) the mutagenic profile for Cas9 and Cas12a-induced DSBs are highly similar, again arguing that repair pathways usage in *Arabidopsis* is grosso modo independent of whether the DNA ends are blunt or have small 5′ protrusions.

Polλ contributes to NHEJ repair of Cas9- and Cas12a-induced DSBs

Cas9-induced DSBs mostly have blunt ends, but instead occasionally have 1-nucleotide 5′-protruding ends (Shou et al., 2018; Zuo & Liu, 2016). The presence of 1 bp insertions following Cas9 DSB induction (Figures 1 and 3), found not only in plants (Fauser et al., 2014; Schmitz et al., 2020; Přibylová et al., 2022) but also in various other species (e.g., Allen et al., 2019), has been proposed to be the consequence of fill-in synthesis of DSBs with such 1-nucleotide 5′-protruding ends. In human cells, this fill-in reaction is mediated by the X-family DNA polymerases λ and μ (Lieber, 2023), and in yeast by the sole X-family DNA polymerase called Pol4 (Lemos et al., 2018), which thus can act to facilitate NHEJ (Mehryar et al., 2023). *Arabidopsis* only encodes one X-family DNA polymerase, called Polλ (Roy et al., 2011; Furukawa et al., 2015), making this protein a logical candidate for this specific mutational outcome. To experimentally test this prediction, and also to address the potential role for NHEJ polymerases on the 4 bp 5′ overhangs produced by Cas12a, we assayed plants containing T-DNA insertion mutations at two different positions in the Polλ gene (Figure 4a). Indeed, in the *polλ* mutants we observed changes in the profiles obtained, especially a great reduction in 1 bp insertions following Cas9-induced DSB (Figure 4b,c). In the PPO locus, these constitute 28% of the mutagenic outcomes for wild type versus only 2% in *polλ* mutant plants. In the ADH locus, the fraction 1 bp insertions was reduced from almost 60% to less than 0.5% in the *polλ* mutants (Figure S3). We also found a decrease of 2 bp insertions (1.3% and 0.25% for wild type and *polλ* mutant plants, respectively), which argues that also 2 bp overhangs, sporadically produced by Cas9, are repair substrates for Polλ-mediated NHEJ. The repair profiles of *polλ* mutant also revealed more subtle deviations, such as a profoundly larger fractions of a specific AT deletion product and a 14 bp deletion product (TTGGCGGGTCTACA; having 5 bp MH) (Figure 4d).

Interestingly, by expanding our analysis to other sequence contexts (by targeting other loci; Figure 4f), we noticed something peculiar: while the vast majority of outcomes at the PPO locus was an insertion of a T nucleotide, consistent with the 1 bp fill-in hypothesis (Figure 4e), other loci had a more diverse spectrum: next to a dominant outcome reflecting fill-in synthesis (a C at the ADH locus, a G at the CRU locus, and an A at the PDS locus; Schmitz et al., 2020; Figure 4f), we found >30% of 1 bp insertions to be a T for all loci tested (Figure 4g). Remarkably, both outcomes are dependent on Polλ presence (Figure 4h). This could point to two activities of Polλ: templated polymerase action filling-in 5′-protrusive ends with the complementary nucleotide and non-templated terminal transferase action adding a nucleotide to blunt ends with a preference for T. The minute level of insertional mutagenesis in *polλ* mutant plants was again consistent with fill-in synthesis of 1 bp

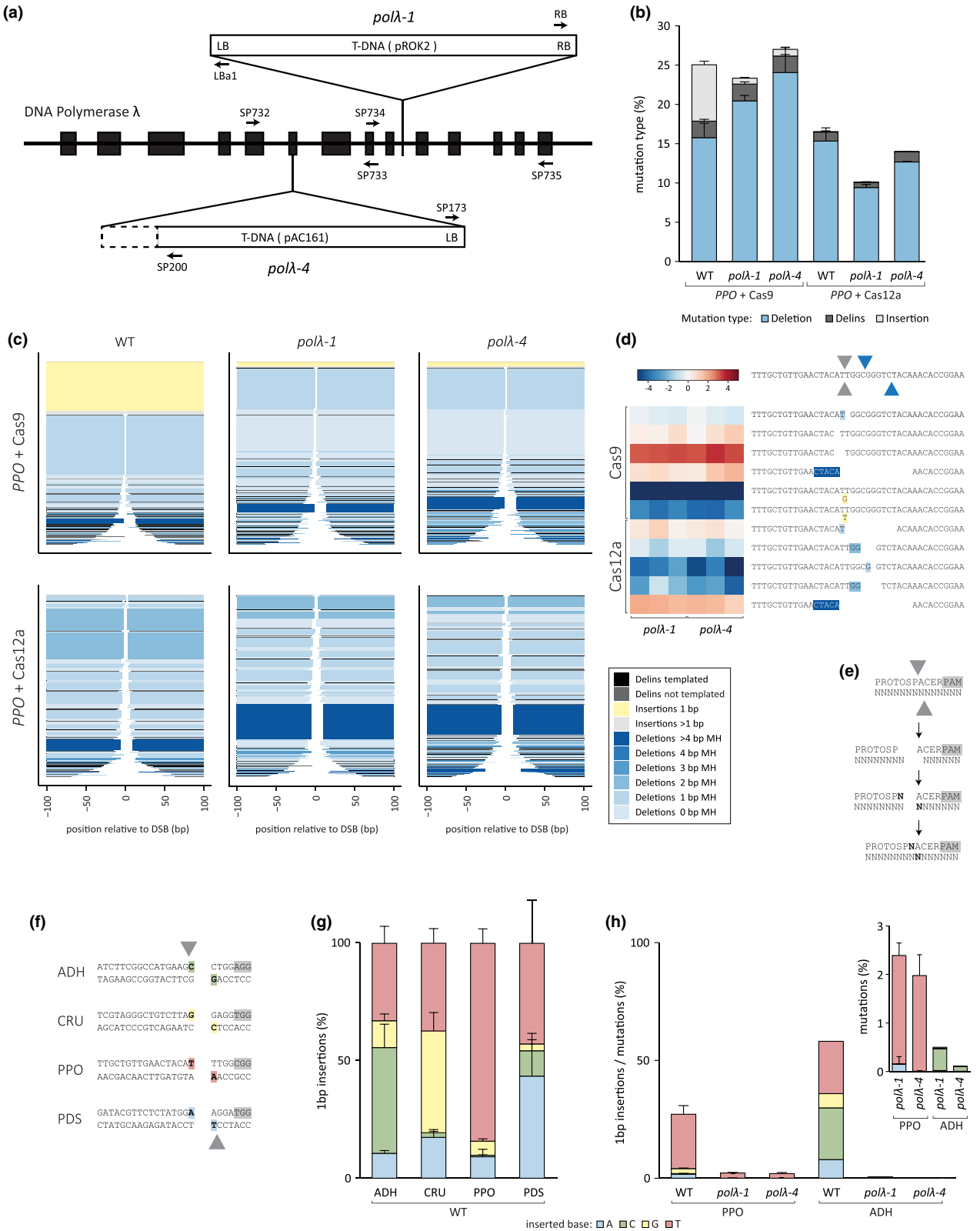

Figure 4. Mutational footprints in wild type, *polλ-1 and polλ-4* mutants.
(a) Structure of the T-DNA insertions in the *polλ-1* (SALK_075391) and *polλ-4* (GABI422E09) mutants. Primers used to genotype the *polλ-4* T-DNA insertion line are indicated.
(b) Percentage of mutagenic reads and their type in wild type, *polλ-1* and *polλ-4* mutants. Error bars represent the standard error of the mean.
(c) Tornado plots of repair footprints of DSBs induced by of Cas9 or Cas12a in the PPO target in wild type, *polλ-1* and *polλ-4* mutants. All mutational events of combined biological replicates are stacked and sorted based on their deletion size. The frequency of occurrence of each event is represented by the thickness of the respective bar. The events are color coded based on the type of event. The relative position on the x-axis includes the expected DSB position at 0 bp.
(d) Heatmap of repair outcomes after Cas9 or Cas12a DSB induction in the PPO target in *polλ* mutants versus wild type. The undigested sequence and mutational outcomes with the largest differences between wild type and mutants are shown on the right. The fold difference between wild type and mutant in occurrence of each mutational outcome is color-coded and shown at the left. The experiment was performed in triplicate.
(e) Filling-in of staggered ends generated by Cas9.
(f) Sequences of the target sites in the Arabidopsis genes ADH, CRU, PPO and the *N. benthamiana* gene PSD (Schmitz et al., 2020). The 1 bp insertion after filling-in the Cas9-induced overhang indicated are colored and the PAM is in gray.
(g) One bp insertion distribution in ADH, CRU, PPO and PDS targets in the wild type.
(h) One bp insertion distribution in the PPO and ADH target in WT, polλ-1 and polλ-4 mutants. Data of the ADH target site are from 1 biological replicate. Zoomed in inset of 1 bp insertion in polλ-1 and polλ-4 is shown.

staggered Cas9 cleavage (a T at the target site in PPO locus, but a C for ADH).

Although Polλ facilitates NHEJ repair of Cas9-induced DSBs with 1 and 2 bp 5′ protrusions through fill-in, it does not perform similarly on the DSBs with 4 bp 5′ protrusions created by Cas12a: in Polλ proficient wild-type plants no 4 bp insertions were found. Nevertheless, we were surprised to find that Polλ deficiency quite significantly changed the mutation profile. As can be concluded from both the tornado plots displayed in Figure 4c as in the top hits visualized in Figure 4d, Polλ is critical for a number of specific NHEJ outcomes.

DISCUSSION

Primarily because of historical reasons, Cas9 is the nuclease of choice in the vast majority of studies. However, other Cas enzymes, most notably Cas12a, are also becoming popular for both methodological reasons—the T-rich PAM sequence substantially expands the range of the target sites—and practical reasons: its usage is free from IP licenses. Adding to its popularity, some studies have reported a greater efficiency for Cas12a than for Cas9 in gene-targeting experiments, across a range of plant species (Wolter & Puchta, 2019; Van Vu et al., 2020; Li et al., 2020). Despite the growing utilization of Cas12a, a comprehensive investigation into the mutational outcomes resulting from repair of Cas12a-induced DSBs in plants had been notably lacking.

In response, we established extensive and detailed mutational profiles induced by Cas12a and drew comparisons with the outcomes induced by Cas9. Remarkably, we observed that both Cas9 and Cas12a exhibited a similar distribution in the contribution of distinct end joining pathways, with approximately 30% of repairs attributed to TMEJ and 70% to NHEJ. In terms of overall efficiency, the LbttCas12a variant used in our experiments (with three different target sites) proved to be on par with Cas9. Other groups also reported similar efficiencies of end-joining generated mutations with Cas9 and Cas12a although different GT frequencies were found (Wolter & Puchta, 2019; Van Vu et al., 2020). The mutation spectra derived from 3 target sites showed subtle differences (Figure S1), which is not unexpected as the availability of micro-homologies is sequence context dependent. Of note, the potentially available micro-homologous sequences exposed by the staggered cutting of Cas12a will not be used in TMEJ as this end joining mechanism acts on 3′ protruding tails, not on 5′ overhangs. Resection thus needs to precede TMEJ for both Cas9 and Cas12a enzymes.

The most noteworthy divergence between the two nucleases was the unique presence of 1 bp insertions in Cas9 spectra, which predominantly results from Polλ-mediated fill-in synthesis of 1 bp staggered-breaks, that can be the result of Cas9 cleavage. In both animal and yeast cells, the predominant type of such single-base insertions typically comprises a repetition of the PAM-distal base (Allen et al., 2019; Lemos et al., 2018). However, we here demonstrate that next to accurate fill-in synthesis also another activity by Polλ contributes to the mutagenesis: 50% to 60% of the 1 bp insertions at these locations consisted of alternative bases, with the vast majority being thymine (T). This outcome could reflect a product of terminal deoxyribonucleotidic transferase activity (TdT) of Polλ (Maga et al., 2005). Apart from establishing fill-in synthesis, also other NHEJ outcomes are affected by Polλ activity as the distribution of specific deletion alleles are different in Polλ proficient versus deficient conditions; the latter also holds true for mutant alleles following Cas12a cleavage. Thus, although both CRISPR enzymes produce categorically distinct DSB configuration, for both of these Polλ aids the repair of a significant fraction. This observation brings about an important notion concerning the efforts to infer details of DNA repair mechanism from mutational outcomes: repair of CRISPR-induced DSB, particularly NHEJ and TMEJ, is often conceptualized (or depicted in mechanistic models) as if the pathway-specific enzymes directly act upon the molecules produced by endonucleolytic cleavage. However, these ends are not necessarily stable

or recalcitrant to exonucleolytic cellular activities. Polλ's involvement in NHEJ of Cas12a-induced DSBs, for instance, may be after few bases are lost at the DSB end—explaining its involvement also in generation of deletion products.

Similarly, the unexpectedly large fraction of large deletions resulting from TMEJ action suggests extensive loss of DNA prior to the action of Polθ, which subsequently uses minute stretches of complementary bases in 3′ ssDNA to anneal and kickstart TMEJ (explaining the MH observed at TMEJ junctions). However, we favor another explanation for the extensive loss of DNA sequence, which may also explain the fact the many deletions have lost DNA only on one end of the DSB: conversion of a DSB into broken sister chromatids by the action of DNA replication. We envision a scenario where a subset of DSBs are induced prior to DNA replication (either in the G1-phase of the cell cycle or in S-phase prior to the target being replicated), but not timely repaired before the replication fork encounters the broken ends. In such a scenario, replication converts the DSB in pre-replicative DNA into DSBs in both sister chromatid, especially if one envisages a converging replication fork approach the site from the opposite direction. In this scenario, four, instead of two DSB ends are in need of DNA repair and HR cannot provide a solution as both sisters are broken (thus no undamaged template available). Two of these four DSB ends have 3′ ends of the original DNA duplex but have served as lagging strands of DNA replication, whereas two novel 3′ ends are generated by leading strand DNA synthesis. It is tempting to speculate that these four ends are not identical and that repair of leading to leading, leading to lagging, and lagging to lagging explains why we observe 3 different categories of TMEJ deletions: limited loss at both ends, substantial loss at one end but not the other, and substantial loss at both ends. The likelihood of such scenario is logically increased in an NHEJ deficient background, as NHEJ repair cannot act and TMEJ has recently been shown to act in post replicative stages of the cell cycle (G2/M) (Brambati et al., 2023; Gelot et al., 2023). Also, error-free NHEJ, which can lead to cycles of cutting and repair, could lead to DSB persistence in S-phase. Finally, the slow off-rate of Cas enzymes may shield the broken DNA strands from DSB recognizing enzymes until a DNA metabolizing machinery, such as the replication fork, displaces all DNA bound proteins. In all these cases, DNA replication, producing new substrates, precedes TMEJ.

Finally, we have addressed the question whether Cas12a-induced breaks are better, worse or equally reactive towards exogenously provided DNA in the form of T-DNA, and found quite similar frequencies and genetic requirements as with Cas9-induced breaks. We thus conclude that both enzymes are effective in genome engineering approaches and that a choice between them can be dictated by other criteria such as the availability of useful PAM sequences in the target locus, or in case of commercial agricultural development by the availability to use reagents and technologies unrestricted by intellectual property rights.

EXPERIMENTAL PROCEDURES

Plant lines

All lines used in this study are derived from the Columbia-0 ecotype. T-DNA insertion lines *teb-5* (SALK_018851) (Van Kregten et al., 2016; Inagaki et al., 2006), *ku70* (SALK_123114) (Jia et al., 2012) and *polλ-1* (SALK_075391) (Roy et al., 2011) were obtained from the SALK institute T-DNA collection (Alonso et al., 2003). *polλ-4* mutant line (GABI422E09) was obtained from the GABI-kat T-DNA insertion line collection (Kleinboelting et al., 2012). The T-DNA insertion in this line is in the 6th exon as determined using genomic primers SP732 and SP733 combined with LB primer SP173 (Table S1). The other junction could not be determined since no PCR product was found using SP732 with either the LB primer (SP173) or the RB primer (SP200) (Figure 4). The junctions were Sanger sequenced: *polλ-1* LB ctcatcttcctgcgttagtttcctTATACTGTTTACTTAAGGGAGTCAGTTCCAAACACTGATAGTTTAAACTGAA; *polλ-1* RB TTGTTTACACCACAATATATCCTGACCCgtttacttaaactgttttttcttatt; *polλ-4* LB CCATTTACAATTGAATATATCCTGGACAAaagcttgaacattttgaaacagat (with T-DNA in capitals and filler DNA underlined).

Agrobacterium tumefaciens strains

All Cas12a constructs used in this study were based on pDE-ttLbCas12a (Schindele & Puchta, 2020) containing a T-DNA sequence with *ttLbCas12a*. The *SpeI-PmeI* fragment containing the gentamicine resistance gene was replaced by the *SpeI-PmeI* fragment containing the phosphinotricin (PPT) resistance gene from pDE-LbCas12a. Oligos (Table S1) were annealed and cloned between the *Bbs*I sites of pEN-RZ-Lb-Chimera to form a crRNA expression cassette, which were inserted in pDE-ttLbCas12a-ppt by Gateway cloning. Final plasmids were checked by Sanger sequencing.

All Cas9 constructs were based on pDE-Cas9 (Fauser et al., 2014). pDE-CasPPO, containing a protospacer specific to the protoporphyrinogen oxidase gene (At4G01690), was constructed and described previously (Shen et al., 2017). pDE-CasCRU, targeting the cruciferin 3 gene (At4G28520) and pDE-CasADH, targeting alcohol dehydrogenase 1 gene (At1G77120) were constructed by (Strunks, 2019). Using electroporation (Den Dulk-Ras & Hooykaas, 1995), constructs were introduced in the disarmed hypervirulent *Agrobacterium tumefaciens* strain AGL1 (Lazo et al., 1991).

Root transformation

Root transformations were performed as described (Vergunst et al., 1998).

Amplicon deep sequencing

Footprint analysis by amplicon deep sequencing and CISGUIDE was performed as described (Kamoen et al., 2024). For PacBio sequencing, 5′ amino modifier C6 (5AmMC6)-modified primers (IDT) were designed to yield products of roughly 4 kb. Library preparation was as described previously (van Schendel et al., 2022), except that PCR amplification was performed with

Phusion polymerase (Thermo Fisher). Sequencing on SequelII was done by Leiden Genome Technology Center (LGTC, Leiden, The Netherlands). NGS data were analyzed using the SIQ software (van Schendel et al., 2022). At least 3 biological replicates were analyzed unless stated otherwise.

For the heatmap (Figure 4d), 5 or 6 outcomes with the largest difference between mutant and wild-type were selected out of the top 10 events observed in the wild type.

AUTHOR CONTRIBUTIONS

SdP, LK, PJJH, and MT conceived the study. SdP and LK conducted experiments. RvS performed bioinformatic analyses. SdP, LK and MT wrote the manuscript with input from all authors, who read the manuscript and authorized its publication.

ACKNOWLEDGEMENTS

We thank the Genome Editing team of Trait Research, BASF Innovation Center Gent (Belgium) for fruitful discussions and for funding parts of this research. We thank Kim Roos, Felix Roelfsema, Rianka Eertink, Loïs Gall for technical assistance and Dr. Holger Puchta for generously providing reagents.

CONFLICT OF INTEREST STATEMENT

The authors declare that there are no conflicts of interest.

DATA AVAILABILITY STATEMENT

Data that support the findings of this study are available within the article and its supplementary material, and openly available from NCBI SRA PRJNA 1117079. Data used for CISGUIDE analysis of Cas9-induced profiles (Kamoen et al., 2024) are available from NCBI SRA PRJNA885005.

SUPPORTING INFORMATION

Additional Supporting Information may be found in the online version of this article.

Figure S1. Tornado plots of repair footprints of DSBs induced by Cas12a in ADH, CRU and PPO targets in wild type, *ku70* and *teb* mutants.

Figure S2. Tornado plots of repair footprints of DSBs induced by of Cas9 in the CRU target in wild type and the *ku70* mutant determined by PacBio.

Figure S3. Mutational footprints in wild type, *polλ-1 and polλ-4* mutants in the ADH target.

Table S1. Primers for genotyping, gRNA cloning and PCR.

Figure S1-S3. Captions

REFERENCES

Allen, F., **Crepaldi, L.**, **Alsinet, C.**, **Strong, A.J.**, **Kleshchevnikov, V.**, **De Angeli, P.** ***et al.*** (2019) Predicting the mutations generated by repair of Cas9-induced double-strand breaks. *Nature Biotechnology*, **37**, 64–82.

Alonso, J.M., **Stepanova, A.N.**, **Leisse, T.J.**, **Kim, C.J.**, **Chen, H.**, **Shinn, P.**, ***et al.*** (2003) Genome-wide insertional mutagenesis of arabidopsis thaliana. *Science*, **301**(5633), 653–657. https://doi.org/10.1126/science.1086391

Bandyopadhyay, A., **Kancharla, N.**, **Javalkote, V.S.**, **Dasgupta, S.** & **Brutnell, T.P.** (2020) CRISPR-Cas12a (Cpf1): a versatile tool in the plant genome editing tool box for agricultural advancement. *Frontiers in Plant Science*, **11**, 1–17.

Bortesi, L. & **Fischer, R.** (2014) The CRISPR/Cas9 system for plant genome editing and beyond. *Biotechnology Advances*, **33**, 41–52.

Brambati, A., **Sacco, O.**, **Porcella, S.**, **Heyza, J.**, **Kareh, M.**, **Schmidt, J.C.** ***et al.*** (2023) RHINO directs MMEJ to repair DNA breaks in mitosis. *Science*, **381**, 653–660.

Capdeville, N., **Merker, L.**, **Schindele, P.** & **Puchta, H.** (2021) Sophisticated CRISPR/Cas tools for fine-tuning plant performance. *Journal of Plant Physiology*, **257**, 153332. Available from: https://doi.org/10.1016/j.jplph.2020.153332

Capdeville, N., **Schindele, P.** & **Puchta, H.** (2023) Getting better all the time—recent progress in the development of CRISPR/Cas-based tools for plant genome engineering. *Current Opinion in Biotechnology*, **79**, 102854. Available from: https://doi.org/10.1016/j.copbio.2022.102854

Chang, H., **Nicholas, P.**, **Noritaka, A.** & **Lieber, M.** (2017) Non-homologous DNA end joining and alternative pathways to double-strand break repair. *Nature Reviews. Molecular Cell Biology*, **18**, 495–506. Available from: https://doi.org/10.1038/nrm.2017.48

Den Dulk-Ras, A. & **Hooykaas, P.J.J.** (1995) Electroporation of Agrobacterium tumefaciens. In: *Plant cell electroporation an electrofusion protocols*. Netherlands: Springer, pp. 63–72.

Fauser, F., **Schiml, S.** & **Puchta, H.** (2014) Both CRISPR/Cas-based nucleases and nickases can be used efficiently for genome engineering in *Arabidopsis thaliana*. *The Plant Journal*, **79**, 348–359.

Furukawa, T., **Angelis, K.J.** & **Britt, A.B.** (2015) Arabidopsis DNA polymerase lambda mutant is mildly sensitive to DNA double strand breaks but defective in integration of a transgene. *Frontiers in Plant Science*, **6**, 357.

Gelot, C., **Kovacs, M.T.**, **Miron, S.**, **Mylne, E.**, **Haan, A.**, **Boeffard-Dosierre, L.** ***et al.*** (2023) Polθ is phosphorylated by PLK1 to repair double-strand breaks in mitosis. *Nature*, **621**, 415–422.

Guo, Y., **Zhao, G.**, **Gao, X.**, **Zhang, L.**, **Zhang, Y.**, **Cai, X.** ***et al.*** (2023) CRISPR/Cas9 gene editing technology: a precise and efficient tool for crop quality improvement. *Planta*, **258**, 36.

Hur, J.K., **Kim, K.**, **Been, K.W.**, **Baek, G.**, **Ye, S.**, **Hur, J.W.** ***et al.*** (2016) Targeted mutagenesis in mice by electroporation of Cpf1 ribonucleoproteins. *Nature Biotechnology*, **34**, 807–808.

Inagaki, S., **Suzuki, T.**, **Ohto, M.**, **Urawa, H.**, **Horiuchi, T.**, **Nakamura, K.** ***et al.*** (2006) Arabidopsis TEBICHI, with helicase and DNA polymerase domains, is required for regulated cell division and differentiation in meristems. *Plant Cell*, **18**, 879–892.

Jia, Q., **Bundock, P.**, **Hooykaas, P.J.J.** & **Pater, S.d.** (2012) Agrobacterium tumefaciens T-DNA integration and gene-targeting in *Arabidopsis thaliana* non-homologous end-joining mutants. *Journal of Botany*, **2012**, 1–13.

Jupe, F., **Rivkin, A.C.**, **Michael, T.P.**, **Zander, M.**, **Motley, S.T.**, **Sandoval, J.P.** ***et al.*** (2019) The complex architecture and epigenomic impact of plant T-DNA insertions. *PLoS Genetics*, **15**, 1–25. Available from: https://doi.org/10.1371/journal.pgen.1007819

Kamoen, L., **Kralemann, L.E.M.**, **Van Schendel, R.**, **Van Tol, N.**, **Hooykaas, P.J.J.** & **De Pater, S.** (2024) Genetic dissection of mutagenic repair and T-DNA capture at CRISPR-induced DNA breaks in *Arabidopsis thaliana*. *PNAS Nexus*, **3**, 1–13. Available at:. Available from: https://doi.org/10.1093/pnasnexus/pgae094

Kamp, J.A., **Lemmens, B.B.L.G.**, **Romeijn, R.J.**, **Changoer, S.C.**, **van Schendel, R.** & **Tijsterman, M.** (2021) Helicase Q promotes homology-driven DNA double-strand break repair and prevents tandem duplications. *Nature Communications*, **12**, 1–12.

Kleinboelting, N., **Huep, G.**, **Kloetgen, A.**, **Viehoever, P.** & **Weisshaar, B.** (2012) GABI-Kat SimpleSearch: new features of the *Arabidopsis thaliana* T-DNA mutant database. *Nucleic Acids Research*, **40**, 1211–1215.

Kleinstiver, B.P., **Tsai, S.Q.**, **Prew, M.S.**, **Nguyen, N.T.**, **Welch, M.M.**, **Lopez, J.M.** ***et al.*** (2016) Genome-wide specificities of CRISPR-Cas Cpf1 nucleases in human cells. *Nature Biotechnology*, **34**, 869–874.

Kralemann, L.E.M., **Pater, S.d.**, **Shen, H.**, **Kloet, S.L.**, **Schendel, R.v.**, **Hooykaas, P.J.J.** ***et al.*** (2022) Distinct mechanisms for genomic attachment of the 5′ and 3′ ends of agrobacterium T-DNA in plants. *Nature Plants*, **8**, 526–534.

Lazo, G.R., **Stein, P.A.** & **Ludwich, A.** (1991) A DNA transformation–competent Arabidopsis genomic library in agrobacterium. *Nature Biotechnology*, **9**, 963–967.

Lemos, B.R., **Kaplan, A.C.**, **Bae, J.E.**, **Ferrazzoli, A.E.**, **Kuo, J.**, **Anand, R.P.** ***et al.*** (2018) CRISPR/Cas9 cleavages in budding yeast reveal templated

insertions and strand-specific insertion/deletion profiles. *Proceedings of the National Academy of Sciences of the United States of America*, **115**, E2010–E2047.

Li, B., **Sun, C.**, **Li, J.** & **Gao, C.** (2024) Targeted genome-modification tools and their advanced applications in crop breeding. *Nature Reviews. Genetics*. Available from: https://doi.org/10.1038/s41576-024-00720-2

Li, S., **Zhang, Y.**, **Xia, L.** & **Qi, Y.** (2020) CRISPR-Cas12a enables efficient biallelic gene targeting in rice. *Plant Biotechnology Journal*, **18**, 1351–1353.

Lieber, M.R. (2023) Pol X DNA polymerases contribute to NHEJ flexibility. *Nature Structural & Molecular Biology*, **30**, 5–8.

Liu, Y., **Cottle, W.T.** & **Ha, T.** (2023) Mapping cellular responses to DNA double-strand breaks using CRISPR technologies. *Trends in Genetics*, **39**, 560–574. Available from: https://doi.org/10.1016/j.tig.2023.02.015

Maga, G., **Ramadan, K.**, **Locatelli, G.A.**, **Shevelev, I.**, **Spadari, S.** & **Hübscher, U.** (2005) DNA elongation by the human DNA polymerase λ polymerase and terminal transferase activities are differentially coordinated by proliferating cell nuclear antigen and replication protein a. *The Journal of Biological Chemistry*, **280**, 1971–1981.

Mehryar, M.M., **Shi, X.**, **Li, J.** & **Wu, Q.** (2023) DNA polymerases in precise and predictable CRISPR/Cas9-mediated chromosomal rearrangements. *BMC Biology*, **21**, 1–16. Available from: https://doi.org/10.1186/s12915-023-01784-y

Přibylová, A., **Fischer, L.**, **Pyott, D.E.**, **Bassett, A.** & **Molnar, A.** (2022) DNA methylation can alter CRISPR/Cas9 editing frequency and DNA repair outcome in a target-specific manner. *The New Phytologist*, **235**, 2285–2299.

Ramsden, D.A., **Carvajal-Garcia, J.** & **Gupta, G.P.** (2022) Mechanism, cellular functions and cancer roles of polymerase-theta-mediated DNA end joining. *Nature Reviews. Molecular Cell Biology*, **23**, 125–140.

Roerink, S.F., **Schendel, R.v.** & **Tijsterman, M.** (2014) Polymerase theta-mediated end joining of replication-associated DNA breaks in *C. Elegans*. *Genome Research*, **24**, 954–962.

Roy, S., **Choudhury, S.R.**, **Singh, S.K.** & **Das, K.P.** (2011) AtPolλ, a homolog of mammalian DNA polymerase λ in *Arabidopsis thaliana*, is involved in the repair of UV-B induced DNA damage through the dark repair pathway. *Plant & Cell Physiology*, **52**, 448–467.

Schimmel, J., **van Schendel, R.**, **den Dunnen, J.T.** & **Tijsterman, M.** (2019) Templated insertions: a smoking gun for polymerase theta-mediated end joining. *Trends in Genetics*, **35**, 632–644. Available from: https://doi.org/10.1016/j.tig.2019.06.001

Schindele, P. & **Puchta, H.** (2020) Engineering CRISPR/LbCas12a for highly efficient, temperature-tolerant plant gene editing. *Plant Biotechnology Journal*, **18**, 1118–1120.

Schmitz, D.J., **Ali, Z.**, **Wang, C.**, **Aljedaani, F.**, **Hooykaas, P.J.J.**, **Mahfouz, M.** ***et al.*** (2020) CRISPR/Cas9 mutagenesis by translocation of Cas9 protein into plant cells via the agrobacterium type IV secretion system. *Frontiers in Genome Editing*, **2**, 1–11.

Shen, H., **Strunks, G.D.**, **Klemann, B.J.P.M.**, **Hooykaas, P.J.J.** & **Pater, S.d.** (2017) CRISPR/Cas9-induced double Strand break repair in Arabidopsis non-homologous end-joining mutants. *G3*, **7**, 193–202.

Shou, J., **Li, J.**, **Liu, Y.** & **Wu, Q.** (2018) Precise and predictable CRISPR chromosomal rearrangements reveal principles of Cas9-mediated nucleotide insertion. *Molecular Cell*, **71**, 498–509. Available from: https://doi.org/10.1016/j.molcel.2018.06.021

Slaman, E., **Kottenhagen, L.**, **De Martines, W.**, **Angenent, G.C.** & **De Maagd, R.A.** (2024) Comparison of Cas12a and Cas9—mediated mutagenesis in tomato cells. *Scientific Reports*, **14**, 1–13. Available from: https://doi.org/10.1038/s41598-024-55088-4

Strunks, G.D. (2019) Strategies for improvement of genome editing in *Arabidopsis thaliana*.

Swartjes, T., **Staals, R.H.J.** & **Van Der Oost, J.** (2020) Editor's cut: DNA cleavage by CRISPR RNA-guided nucleases Cas9 and Cas12a. *Biochemical Society Transactions*, **48**, 207–219.

Tang, X., **Lowder, L.G.**, **Zhang, T.**, **Malzahn, A.A.**, **Zheng, X.**, **Voytas, D.F.** ***et al.*** (2017) A CRISPR-Cpf1 system for efficient genome editing and transcriptional repression in plants. *Nature Plants*, **3**, 1–5.

Van Kregten, M., **De Pater, S.**, **Romeijn, R.**, **Van Schendel, R.**, **Hooykaas, P.J.J.** & **Tijsterman, M.** (2016) *T-DNA integration in plants results from Polymerase Theta-mediated DNA repair*. Plants: Nat.

van Schendel, R., **Schimmel, J.** & **Tijsterman, M.** (2022) SIQ: easy quantitative measurement of mutation profiles in sequencing data. *NAR Genomics and Bioinformatics*, **4**, 1–10.

Van Vu, T., **Sivankalyani, V.**, **Kim, E.J.**, **Doan, D.T.H.**, **Tran, M.T.**, **Kim, J.** ***et al.*** (2020) Highly efficient homology-directed repair using CRISPR/Cpf1-geminiviral replicon in tomato. *Plant Biotechnology Journal*, **18**, 2133–2143.

Vergunst, A.C., **de Waal, E.C.** & **Hooykaas, P.J.J.** (1998) Arabidopsis protocols: root transformations by *Agrobacterium tumefaciens*. *Methods in Molecular Biology*, **82**, 227–244.

Wolter, F. & **Puchta, H.** (2019) In planta gene targeting can be enhanced by the use of CRISPR/Cas12a. *The Plant Journal*, **100**, 1083–1094.

Wood, R.D. & **Doublié, S.** (2022) Genome protection by DNA polymerase θ. *Annual Review of Genetics*, **56**, 207–228.

Zhang, Y., **Cheng, Y.**, **Fang, H.**, **Roberts, N.**, **Zhang, L.**, **Vakulskas, C.A.** ***et al.*** (2022) Highly efficient genome editing in plant protoplasts by ribonucleoprotein delivery of CRISPR-Cas12a nucleases. *Frontiers in Genome Editing*, **4**, 1–11.

Zuo, Z. & **Liu, J.** (2016) Cas9-catalyzed DNA cleavage generates staggered ends: evidence from molecular dynamics simulations. *Scientific Reports*, **5**, 1–9.